Monthly Notices
of the
ROYAL ASTRONOMICAL SOCIETY

MNRAS **494,** L75–L80 (2020)
Advance Access publication 2020 March 9

doi:10.1093/mnrasl/slaa039

# Finding binary black holes in the Milky Way with *LISA*

Alberto Sesana,[1]★ Astrid Lamberts[2] and Antoine Petiteau[3]

[1]*Dipartimento di Fisica 'G. Occhialini', Università degli Studi di Milano-Bicocca, Piazza della Scienza 3, I-20126 Milano, Italy*
[2]*Université Côte d'Azur, Observatoire de la Côte d'Azur, CNRS, Laboratoire Lagrange, Laboratoire ARTEMIS, Bd de l'Observatoire, CS 34229, 06304, Nice, Cedex 4, France*
[3]*APC, Université Paris Diderot, CNRS/IN2P3, CEA/lrfu, Observatoire de Paris, Sorbonne Paris Cité, 10 rue Alice Domon et Léonie Duquet, F-75205 Paris Cedex 13, France*

Accepted 2020 February 28. Received 2020 February 28; in original form 2019 December 13

## ABSTRACT

We determine the main properties of the Galactic binary black hole (BBH) population detectable by *Laser Interferometer Space Antenna* (*LISA*) and strategies to distinguish them from the much more numerous white dwarf binaries. We simulate BBH populations based on cosmological simulations of Milky Way-like galaxies and binary evolution models. We then determine their gravitational wave emission as observed by *LISA* and build mock catalogues. According to our model, *LISA* will detect ≈4 (6) BBHs assuming 4 (10) yr of operations. Those figures grow to ≈6 (9) when models are re-normalized to the inferred LIGO/Virgo merger rates. Largely independent on mass and distance, sources emitting at $f > 0.5$ mHz – 40 per cent (70 per cent) of the detections – have a measurable frequency drift, which allows a good enough chirp mass measurement to separate them from the much lighter white dwarf and neutron star binaries. Most of the remaining, lower frequency, sources should be identifiable by their lack of electromagnetic (EM) counterpart within ≈100 pc. These results are robust with respect to the current uncertainties of the BBH merger rate as measured by LIGO/Virgo as well as the global mass spectrum of the binaries. Based on the LIGO/Virgo merger rate, we determine that there is a 94 per cent chance that *LISA* finds at least one of these systems within 4 yr, which will allow us to pinpoint the conditions where they were formed and possibly find unique EM signatures.

**Key words:** gravitational waves – binaries: close – Galaxy: stellar content.

## 1 INTRODUCTION

The detection of gravitational waves (GWs) from merging binary black holes (BBHs) by LIGO/Virgo (Abbott et al. 2019a) raises the crucial question of the origin of the observed events. The first detections reveal a merger rate at the high end of the theoretical predictions (Abbott et al. 2016a, 2019b) and somewhat unexpectedly high BBH masses. These systems likely originate from massive field binary evolution in low-metallicity environments or from *N*-body interactions in dynamical environments such as star clusters (Abbott et al. 2016b). A statistical analysis of larger samples of detections may eventually allow us to distinguish between these formation channels (Zevin et al. 2017). However, given that no electromagnetic (EM) counterpart to BBH mergers has been observed so far, the exact identification of the conditions of the formation of a given merger remains uncertain.

Stellar mass BHs in the Milky Way (MW) have been observed for decades in X-ray binaries. In those systems, the BH is feeding off the companion star, and the presence of an accretion disc, and of a complementary relativistic jet, leads to strong non-thermal emission, from radio to X-rays and sometimes, gamma rays. The masses of the BHs are usually extracted from the Doppler shift in the spectrum of the companion star and found to be between 5 and 10 $M_\odot$ (Corral-Santana et al. 2016), which differs significantly from the currently observed LIGO/Virgo population. Stellar BHs also cause proper motions to their companion star, and their presence can be inferred by astrometric measurements (e.g. Gould & Salim 2002; Breivik, Chatterjee & Larson 2017) or photometric and radial velocity observations (Liu et al. 2019; Thompson et al. 2019) even if no non-thermal emission is observable. A handful of unconfirmed BH candidates come from micro-lensing (Wyrzykowski et al. 2016). Finally, lone BHs can be lightened up by the accretion of the interstellar medium, although no such objects have been observed so far. As such, our inventory of the BH content of the MW remains very sparse and connecting it to the observed BBH mergers is challenging.

The *Laser Interferometer Space Antenna* (*LISA*) will be a space-based GW detector operating between $10^{-5}$ and 1 Hz. Sesana (2016) showed that certain binaries of masses comparable to GW150914

★ E-mail: alberto.sesana@unimib.it

will be observable by *LISA* several months before their merger, and will be mutliband GW sources. *LISA* will also observe stellar mass compact binaries with periods below 1 h within our MW, or nearby galaxies (Korol, Koop & Rossi 2018). The vast majority of these sources will be double white dwarf (DWD), with chirp masses well below 1 $M_\odot$, which will also create an unresolved foreground below a few mHz (Nelemans, Yungelson & Portegies Zwart 2001). Between 30 and 300 signals from binary neutron stars (BNSs) and a handful of BBHs are likely to be present in the data stream as well (Christian & Loeb 2017; Andrews et al. 2019; Lau et al. 2019; Seto 2019).

Using a binary population synthesis model and a cosmological simulation of an MW-like galaxy, Lamberts et al. (2018) showed that roughly a million BBHs are present in the MW. Based on those models, summarized in Section 2, we study in this letter the population of MW BBHs detectable by *LISA*. In Section 3, we describe the properties of those systems and strategies to separate them from the outnumbering population of DWDs (and also from BNSs). Finally, in Section 4, we demonstrate the robustness of our results and discuss the scientific payouts of detecting those sources.

## 2 THE BINARY BLACK HOLE POPULATION OF THE MW

This work is based on the BBH models presented in Lamberts et al. (2018), where all the details about the binary evolution model and the galaxy model can be found. The model is applied to three MW analogues (**m12i**, **m12b**, and **m12c**) from the FIRE simulation suite (Hopkins et al. 2018). The cosmological simulations produce galaxies with their global stellar mass, morphology, metallicity gradients, and population of satellite galaxies comparable to the present-day MW. These models predict that roughly a million BBHs should be currently present in an MW-like galaxy, mostly in the Galactic bulge and stellar halo, as these objects stem from progenitors stars of mean metallicity of 0.25 $Z_\odot$. There is less than a 15 per cent difference in the total number of BBHs present in each of the three model Galaxies, and their global properties (masses, locations, and periods) are the same.

For each of the three galaxies, we generate 100 realizations of the BBH population to assess the statistical uncertainty level in the number of detections due to the stochasticity of the BBH formation process. For each realization, we also randomly choose the phase of the Solar system along its 8 kpc-radius circular orbit in the galactic plane. We start our analysis with 300 BBH catalogues of masses, orbital frequencies, and 3D Cartesian coordinates with respect to a reference frame centred on the present-day Galactic Centre and with the $x$–$y$ plane aligned with the galactic disc mid-plane.

The effect of eccentricity, $e$, on *LISA* source detectability is highly non-linear. Even for moderate values $e \approx 0.1$, the signal is strongly dominated by the second harmonic and the overall source signal-to-noise ratio (SNR) hardly deviates from the circular value. In the field formation scenario, the overwhelming majority of BBHs have $e < 0.1$ in the *LISA* band (Breivik et al. 2016; Nishizawa et al. 2017), and certainly this is the case in our model, in which all detectable systems have $e < 0.1$. Also, in the standard dynamical formation channel, most BBHs have $e < 0.1$ in the *LISA* band, although with a long tail extending to higher frequencies (Breivik et al. 2016; Rodriguez, Chatterjee & Rasio 2016). Although a number of scenarios involving, e.g. field hierarchical triplets (Antonini, Toonen & Hamers 2017), evolution in the tidal field of a massive BH (Antonini & Rasio 2016), and binary–single (Samsing & Ramirez-Ruiz 2017) and binary–binary (Zevin et al. 2019) interactions can result in highly eccentric systems, they are expected to produce a subdominant fraction of the overall BBH population. We therefore consider BBHs to have a negligible eccentricity in our analysis. Under this assumption, the sky-inclination-polarization-averaged SNR for a BBH of frequency $f$ can be approximated as

$$\bar{\rho}^2 = 2\frac{h^2 N}{f\langle S(f)\rangle}, \tag{1}$$

where $N = f \times T$ is the number of observed wave cycles during the *LISA* observing time $T$, $\langle S(f)\rangle = (20/3)S(f)$ is the sky-averaged sensitivity of the detector [$S(f)$ being its intrinsic noise power spectral density], and

$$h = \sqrt{\frac{32}{5}}\frac{(G\mathcal{M}_c)^{5/3}}{c^4 D}(\pi f)^{2/3} \tag{2}$$

is the inclination-polarization-averaged GW strain. The latter is written as a function of the source chirp mass $\mathcal{M}_c = (M_1 M_2)^{3/5}/(M_1 + M_2)^{1/5}$ and distance $D$.

We use equation (1) to select the BBHs with $\bar{\rho} > 1$ in each catalogue, usually between 30 and 100, depending on the realization. To each selected system, we then assign an inclination angle $\iota$, randomly drawn from a uniform distribution $-1 < \cos\iota < 1$, a polarization angle $\psi$, randomly selected between 0 and $\pi$, and an initial orbital phase $\phi_0$, randomly selected between 0 and $2\pi$. From $\mathcal{M}_c$, $D$, and $f$, we can then evaluate the GW amplitude parameter

$$A = 2\frac{(G\mathcal{M}_c)^{5/3}}{c^4 D}(\pi f)^{2/3} \tag{3}$$

and the frequency drift parameter

$$\dot{f} = \frac{96}{5c^5}\pi^{8/3}(G\mathcal{M}_c)^{5/3} f^{11/3}. \tag{4}$$

From the 3D sky localization, we compute the celestial angular coordinates $\theta_s$ and $\phi_s$. Each signal is therefore modelled as a quasi-monochromatic source slowly drifting in frequency and defined by the eight parameters $\vec{\lambda} = (f, \dot{f}, A, \theta_s, \phi_s, \iota, \psi,$ and $\phi_0)$. For each system, the SNR $\rho$ and the uncertainties on each of the parameters $\vec{\lambda}$ are computed with a code using the Fisher matrix approximation, the core infrastructure of the *LISA* Data Challenge[1] and a fast computation of the signal in the frequency domain coupling waveform and instrument response. The Fisher matrix approximation has been checked against the Bayesian samplers, EMCEE (Foreman-Mackey et al. 2013), and Dynesty (Speagle 2019). A foreground from unresolved Galactic DWDs based on the same binary evolution model and same galaxy simulation is included in the analytic expression of the noise.

## 3 RESULTS: BINARY BLACK HOLE DETECTION AND IDENTIFICATION

We mark as 'detected' sources with $\rho > 7$. Based on our 300 mock populations, we expect on average $\bar{N}_4 = 4.2$ and $\bar{N}_{10} = 6.5$ *LISA* detections, assuming mission operations of $T = 4$ and 10 yr, respectively. The distributions are broad and the median and 90 per cent confidence intervals of the number of detections are $N_4 = 3.4^{+4.9}_{-3.0}$ and $N_{10} = 5.8^{+5.7}_{-4.5}$. These numbers differ by only $\approx$10 percent with those estimated using the more crude sky-inclination-polarization-averaged method of equation (1), which yields $\bar{N}_{10} = 5.7$.

Fig. 1 compares the number density distribution of a mock DWD

[1] https://lisa-ldc.lal.in2p3.fr/

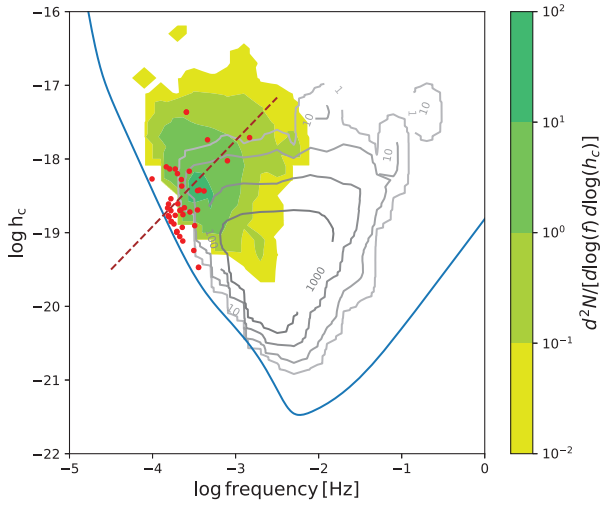


**Figure 1.** Differential density distribution of BBHs (filled green contours, averaged over 300 mock catalogues) and DWDs (open grey contours) in the $f$–$h_c$ plane. For *LISA*, we plot the equivalent strain sensitivity $h_{\rm LISA} = f\langle S(f)\rangle$. The red dots display all sources with $\bar{\rho} > 1$ in a selected BBH population for comparison. The brown-dashed line represents the dependence of the characteristic strain for a persistent monochromatic source as a function of frequency, $h_c = h\sqrt{N} \propto f^{7/6}$. 10 yr of *LISA* operations are assumed.

population with the average number density distribution of observed BBHs from our 300 mock populations in the $f$–$h_c$ space. $h_c = h\sqrt{N}$ is the characteristic strain of the GW. The DWD populations is taken from Lamberts et al. (2019) and is based on the same Galaxy simulation and binary population model as the BBH distribution. The two distributions are clearly different with the DWDs clustering at 1 mHz $< f <$ 10 mHz, with $10^{-20} < h_c < 10^{-19}$, and the BBHs being shifted by an order of magnitude lower in frequency and higher in strain. Nevertheless, the DWD population is much more numerous and it overlaps significantly with the BBH one. All BBHs with $\bar{\rho} > 1$ from a selected realization of the Galaxy are also shown for comparison. However, one system on the left can be safely separated from the DWD population, all the others occupy a portion of the parameter space overlapping with the DWD. We, therefore, need to devise strategies to separate the BBH population from the dominant (number-wise) DWD systems.

The easiest way to confirm the BBH nature of a detected system is the measurement of its chirp mass. However, the parameters $\vec{\lambda}$ of the model do not directly include neither $\mathcal{M}_c$ and $D$, which have to be estimated from equations (3) and (4) via error propagation. Assuming for simplicity no correlation among the errors on the parameters, the uncertainties on distance and chirp mass are

$$\frac{\Delta D}{D} = \sqrt{\left(\frac{2}{3}\frac{\Delta f}{f}\right)^2 + \left(\frac{5}{3}\frac{\Delta \mathcal{M}_c}{\mathcal{M}_c}\right)^2 + \left(\frac{\Delta A}{A}\right)^2}, \quad (5)$$

$$\frac{\Delta \mathcal{M}_c}{\mathcal{M}_c} = \sqrt{\left(\frac{11}{5}\frac{\Delta f}{f}\right)^2 + \left(\frac{3}{5}\frac{\Delta \dot{f}}{\dot{f}}\right)^2}. \quad (6)$$

Fig. 2 shows the expected measurement error distributions for the sky localization $\Delta\Omega$ (a), distance $\Delta D/D$ (b), and chirp mass $\Delta\mathcal{M}_c/\mathcal{M}_c$ (c). $\mathcal{M}_c$ can be reasonably measured for 40 per cent (70 per cent) of the systems for a 4 (10) yr mission. Using equation (6), we estimate a $2\sigma$ lower limit $\mathcal{M}_{c,\rm min} = \mathcal{M}_c - 2\Delta\mathcal{M}_c$, and we separate the detected BBH population in systems with $\mathcal{M}_{c,\rm min} <$ 1.2 $M_\odot$ and systems with $\mathcal{M}_{c,\rm min} >$ 1.2 $M_\odot$. Since 1.2 $M_\odot$ is the typical BNS chirp mass, the latter are systems containing *at least one BH* and we expect on average 1.8 (4.4) of them over a 4 (10) yr mission. The two separate sub-populations are highlighted in panel (d) of Fig. 2, and are marked with dotted and dashed lines, respectively, in all the panels.

The global properties of the detected BBHs (SNR, chirp mass, distance, and frequency) are displayed in Fig. 3, which show that most sources are located 8 kpc away, in the Galactic bulge, and have a frequency of 0.3 mHz, which is ≈10 times lower than the typical frequency at which individual DWDs are detected (Nelemans et al. 2001). Fig. 3 also reveals that BBHs with confident mass measurement are generally detected at higher frequency ($f > 0.5$ mHz, panel d) where they have higher $\rho$ (panel a) because of the shape of the *LISA* sensitivity curve (cf. Fig. 1). At a high frequency, the frequency drift of the signal over the mission lifetime is much larger than *LISA*'s frequency resolution, i.e. $\dot{f} \times T \gg 1/T$, meaning that $\Delta\dot{f}/\dot{f}$ in equation (6) is small and $\mathcal{M}_c$ can be measured with confidence. The direct dependence of this quantity on $T$ explains why $\mathcal{M}_c$ can be estimated for a larger percentage of sources in a 10 yr mission. The actual distance or mass of the source have little impact on the measurability of its $\mathcal{M}_c$ (see Fig. 3). Fig. 2 highlights that systems with measurable $\mathcal{M}_c$ are also those with a better estimate of $\Delta\Omega$ and $\Delta D/D$ (panels a and b), resulting in a fair estimate of the 3D sky location of the source, shown in panel e. For $T = 4$ (10) yr, we typically expect one (two) sources to be localized within 10 deg$^2$. These sources would also have a 3D sky localization within a volume smaller than 1 kpc$^3$.

Establishing the BBH nature of sources below 0.5 mHz is less straightforward and we consider the possibility of identifying them from the lack of an EM counterpart. Due to their sub-solar masses, DWDs must be necessarily close to the Solar system to be individually detectable *LISA* GW sources at $f < 0.5$ mHz. Assuming a loud GW signal with a given $\hat{\rho}$ at $f < 0.5$ mHz, for which we cannot measure $\mathcal{M}_c$, the maximum distance at which the DWD would lie in order to produce an SNR $\hat{\rho}$ is

$$D_{\rm max} = 4\sqrt{\frac{2}{f\langle S(f)\rangle}\frac{(G\mathcal{M}_{\rm DWD})^{5/3}}{c^4\hat{\rho}}(\pi f)^{2/3}}, \quad (7)$$

where we assume a face-on binary, we use the sky-averaged *LISA* sensitivity, and we consider a DWD chirp mass of $\mathcal{M}_{\rm DWD} = 0.5\,M_\odot$, typical for carbon–oxygen WDs which will be the dominant WD population detected by *LISA* at low frequencies (Lamberts et al. 2019). Fig. 4 shows that DWDs producing contaminant GW signals will be within 600 pc, and mostly within 200 pc. Assuming a conservative absolute magnitude for the WD $M_v = 15$ (Gaia Collaboration 2018), the $D_{\rm max}$ distribution can be converted into an apparent magnitude $m_v$

$$m_v = M_v + \log 2 + 5\log\left(\frac{D_{\rm max}}{10\,\rm pc}\right), \quad (8)$$

where the log 2 factor accounts for the fact that there are two WDs in a binary and we ignore extinction because of the proximity of the sources (Capitanio et al. 2017). Fig. 4 shows the apparent magnitude distribution that can be compared to the *Gaia* and LSST flux limits. Thanks to a single-point flux limit of 20.7, the *Gaia* catalogue is expected to be complete for WDs up to 60 pc (Gentile Fusillo et al. 2019) beyond that the oldest WDs may not be detected due to their lower temperatures. About three quarters of the DWDs with GW frequencies between $10^4$ and $4 \times 10^{-4}$ Hz are less than 3 Gyr old. As such, their luminosity has not faded too strongly for them to be observable at much larger distances (Carrasco et al. 2014). For the He–He DWDs, this fraction may be lower but these

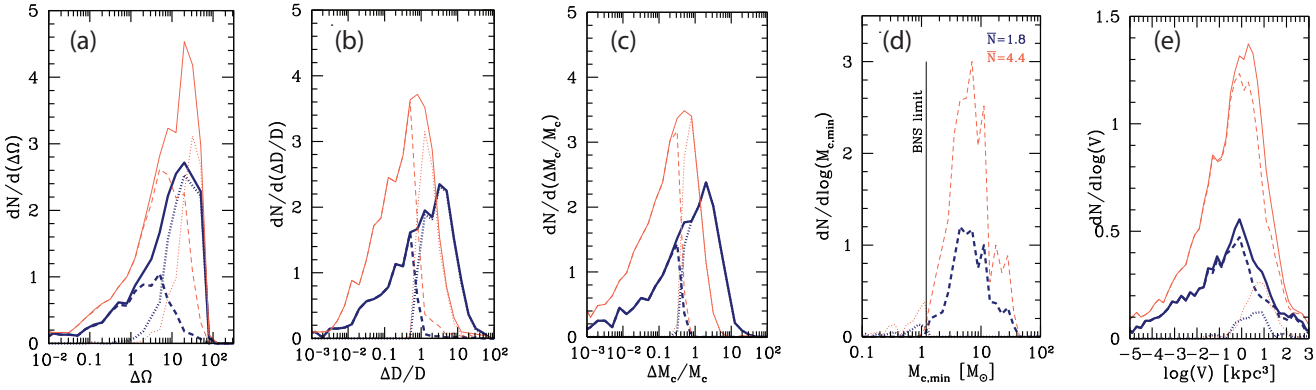


**Figure 2.** Measurement uncertainties of the sky localization (a), distance (b), and chirp mass (c) of the BBHs, averaged over 300 mock catalogues. Panel (d) shows the distribution of $\mathcal{M}_{\rm c,min}$ estimates (see text for details), separated in systems with $\mathcal{M}_{\rm c,min} < 1.2\,{\rm M}_\odot$ (dotted) and $\mathcal{M}_{\rm c,min} > 1.2\,{\rm M}_\odot$ (dashed). Note that the dotted curves have a spike at $\mathcal{M}_{\rm c,min} = 0$, which is not shown in panel (d). The two sub-populations are reported in all panels (dotted and dashed lines) together with the overall population (solid lines). Panel (e) shows the distribution of 3D volume localization, note that systems with $\mathcal{M}_{\rm c,min} = 0$ do not have distance determination, resulting in $V = \infty$ (not shown). Linestyle as in Fig. 3. Thick-blue (thin-red) lines are for 4 (10) yr of *LISA* operations.

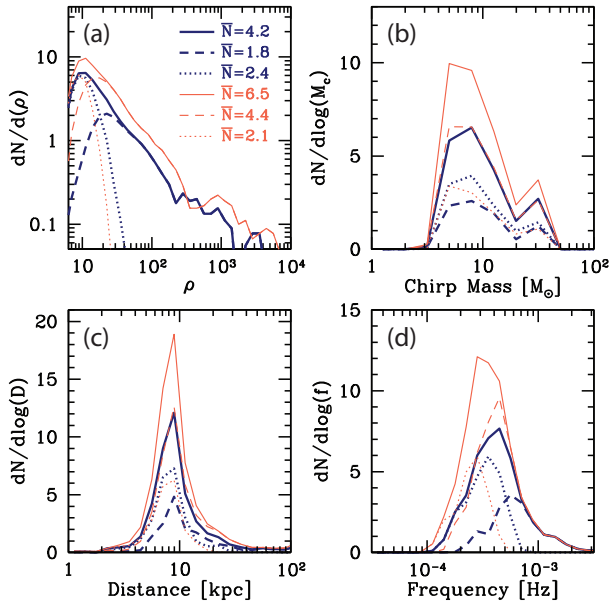


**Figure 3.** Properties of detected BBHs averaged over 300 galaxy mock realizations: distributions of SNR (a), chirp mass (b), distance to the Sun (c), and GW frequency (d). Linestyle as in Fig. 2.

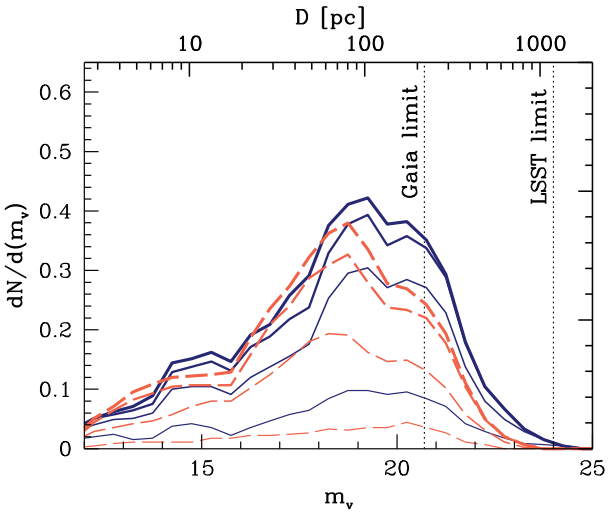


**Figure 4.** Magnitude (bottom label) and distance (top label) distributions of putative DWDs producing a GW signal equivalent to that generated by the observed BBHs. Only systems at $f < 0.5$ mHz for which $\mathcal{M}_{\rm c}$ cannot be measured are considered. The solid-blue and dashed-red lines are for 4 and 10 yr of *LISA* operations, respectively. Lines from bottom to top, in order of increasing thickness, identify systems that can be localized within 10, 30, 50, and 100 deg$^2$.

WDs are intrinsically brighter due to their larger radius and may be more subject to tidal heating for the same reason. With its ≈24 mag single-point flux limit, LSST is expected to detect WDs out to ≈1kpc. Proper identification, however, will likely require deep spectroscopic follow-ups. Globally we expect that most, if not all the nearby DWD binaries with periods of a few hours will be detected electromagnetically by the time *LISA* flies.

The difficulty will be to associate the *LISA* sources with the WDs from EM, the source catalogues. The very short-period binaries we consider will not be resolved by *Gaia* and their binary nature will be unknown. Fig. 4 shows that about 50 per cent of them are located by *LISA* in the sky with $\Delta\Omega \approx 30\,{\rm deg}^2$, which corresponds to a volume of $\approx 10^4\,{\rm pc}^3$ at 100 pc. Given the local WD density (including singles and multiples) of $5 \times 10^{-3}$ pc$^{-3}$ (Holberg et al. 2016), there will be roughly 50 WDs within the uncertainty region defined by *LISA*. For the least well localized sources, the uncertainty region may contain hundreds of WDs. As such, additional information will be necessary to identify the exact counterpart. Preliminary selection could be done based on the *Gaia* colour–magnitude diagram, ruling out the coldest and oldest stars and possibly subselecting binaries, which are brighter for a given colour. Formal identification of a counterpart will require the measurement of a binary period. Such information could be based on the final *Gaia* light curves (Korol et al. 2017), follow-up multifibre spectroscopic surveys such as WEAVE (Dalton et al. 2014), 4MOST (de Jong et al. 2014), or SDSS-V (Kollmeier et al. 2017) or light curves from high-cadence surveys such as ZTF (Bellm et al. 2019) or LSST for the faintest systems. Given appropriate search strategies, we expect that by the end of the *LISA* mission, the identification of appropriate EM counterparts to unidentified low-frequency systems will be feasible.

The lack of a plausible DWD candidate would strongly support the BBH nature of the system. DNSs are expected to be rare and unlikely to be detected at $f \lesssim 0.3$ mHz (Andrews et al. 2019; Breivik et al. 2019). The same is generally true for NS–BH systems that may be more difficult to separate from the BBH population. In any case, we can say with confidence that, in absence of a counterpart, the system contains at least one BH.

## 4 DISCUSSION AND CONCLUSIONS

We based our study on the BBHs found in the three MW-equivalent galaxies, which have a BBH merger rate $\approx 8 \times 10^{-6}$ yr$^{-1}$. Assuming an MW-equivalent volume density of 0.005 Mpc$^{-3}$ (Tomczak et al. 2014), this results in a BBH merger rate at $z = 0$ of 40 yr$^{-1}$ Gpc$^{-3}$, which is consistent with the measured LIGO-Virgo rate of $53^{+58}_{-29}$ yr$^{-1}$ Gpc$^{-3}$ (Abbott et al. 2019b). To fold into our calculation, the uncertainties in the measured BBH rate, we convolve the distribution of expected detections with the posterior distribution of the LIGO/Virgo merger rate and we find an average number of detections of $\bar{\mathcal{N}}_4 = 6.1$ and $\bar{\mathcal{N}}_{10} = 9.3$. The distributions are highly asymmetric and the median and 90 per cent confidence intervals of the number of detection are $\mathcal{N}_4 = 4.8^{+10.7}_{-4.0}$ and $\mathcal{N}_{10} = 7.7^{+14.8}_{-5.8}$. The probability of *LISA* detecting *at least* one *BBH* is 0.94 and 0.99 in the two cases. This prediction holds under the assumption that the dominant BBH formation channel is binary field evolution. A significant contribution from a range of dynamical channels might in fact produce very eccentric binaries, resulting in sparser sources in the *LISA* band (e.g. Nishizawa et al. 2017).

We also investigated how our results depend on the model of the BBH chirp mass distribution. Naively, a factor of 2 difference in $\mathcal{M}_c$ would result in a factor of >3 increase in the maximum distance of observable sources and thus in a factor of ≈30 difference in the number of detected systems. This is in general not the case, as we shall now demonstrate. In all cases, the merger rate has to satisfy the LIGO constraint. Since $\mathrm{d}n/\mathrm{dln}f = (\mathrm{d}n/\mathrm{d}t)(\mathrm{d}t/\mathrm{dln}f)$, at a fixed rate, the number of binaries per unit log frequency is proportional to the time they spend at that frequency, i.e. $\mathrm{d}t/\mathrm{dln}f \propto f^{-8/3}\mathcal{M}_c^{-5/3}$ (cf. equation 4). It results that the number of detectable sources is set by the lowest observable frequency $f_{\rm min}$. Let us consider a source at a given distance; its characteristic strain integrated over the observation time is $h_c = h\sqrt{N} \propto f^{7/6}\mathcal{M}_c^{5/3}$ – cf. equation (2) – as represented by the dashed-brown line in Fig. 1. The line intersects the sensitivity curve at a frequency $f_{\rm min}$, that depends on the considered source and chirp mass. Since $h_c \propto f^{7/6}\mathcal{M}_c^{5/3}$ and the *LISA* sensitivity in the relevant frequency range is $h_{\rm LISA} \propto f^{-2}$, by taking the log of the two expressions and equating them, one gets $\log f_{\rm min} \propto -(10/19)\log\mathcal{M}_c$. Since $\log N \propto -(8/3)\log f - (5/3)\log\mathcal{M}_c$, this gives $\log N \propto -(15/57)\log\mathcal{M}_c$. This means that a change in chirp mass by a factor of 2 only changes the number of detected events by about 20 per cent. To test this, we artificially multiplied the chirp mass of all the BBHs in our catalogue by a factor $\alpha$ (reweighting them by a factor $\alpha^{-5/3}$ in order to preserve the merger rate) and we computed the number of *LISA* detections. Even when we varied $\alpha$ by almost two orders of magnitude, the number of detected sources was close to our current model for both 4 and 10 yr *LISA* mission. We, therefore, conclude that the number of detections estimated here are robust and only mildly dependent on the detailed properties of the BBH mass distribution.

On the other hand, we stress that this is valid under the assumption that $\mathrm{d}t/\mathrm{dln}f \propto f^{-8/3}$, which is strictly valid only for circular systems. Highly eccentric binaries would be sparser, resulting in fewer detections. Nonetheless, standard BBH formation scenarios result in eccentricity generally lower than 0.1 in the *LISA* band, which will not affect the results of our analysis.

The detection of Galactic BBHs therefore sets another important goal of the *LISA* mission. The determination of their chirp mass and 3D localization within the MW might provide important clues about their origin, and their connection to other galactic BHs found in X-ray binaries. With this goal in mind, we stress the importance of an extended *LISA* lifetime. When normalized to the LIGO/Virgo merger rate 10 yr of *LISA* operations will allow the detection of $\mathcal{O}(10)$ binaries, and relevant parameter measurements for the majority of them. Finally, with $\mathcal{O}(1)$ system localized within 1 deg$^2$, the *LISA* Galactic BBH detections may also offer the first opportunity to observe any EM counterpart to isolated BHs, including radio observations with SKA or X-ray observations with the *Wide Field Imager* onboard of *Athena* satellite.

## ACKNOWLEDGEMENTS

This research was supported in part by the National Science Foundation under Grant No. NSF PHY-1748958. AS is supported by the ERC through a CoG grant. AL acknowledges support by the Programme National des Hautes Energies (France). AP and AL acknowledge support by the Centre National d'Etudes Spatiales. The authors acknowledge the *LISA* Data Challenge Team that developed the core part of the code used for parameter estimations.

## REFERENCES

Abbott B. P. et al., 2016a, ApJS, 227, 14
Abbott B. P. et al., 2016b, ApJ, 818, L22
Abbott B. P. et al., 2019a, Phys. Rev., X9, 031040
Abbott B. P. et al., 2019b, ApJ, 882, L24
Andrews J. J., Breivik K., Pankow C., D'Orazio D. J., Safarzadeh M., 2019, preprint (arXiv:1910.13436)
Antonini F., Rasio F. A., 2016, ApJ, 831, 187
Antonini F., Toonen S., Hamers A. S., 2017, ApJ, 841, 77
Bellm E. C. et al., 2019, PASP, 131, 018002
Breivik K., Rodriguez C. L., Larson S. L., Kalogera V., Rasio F. A., 2016, ApJ, 830, L18
Breivik K., Chatterjee S., Larson S. L., 2017, ApJ, 850, L13
Breivik K. et al., 2019, preprint (arXiv:1911.00903)
Capitanio L., Lallement R., Vergely J. L., Elyajouri M., Monreal-Ibero A., 2017, A&A, 606, A65
Carrasco J. M., Catalán S., Jordi C., Tremblay P. E., Napiwotzki R., Luri X., Robin A. C., Kowalski P. M., 2014, A&A, 565, A11
Christian P., Loeb A., 2017, MNRAS, 469, 930
Corral-Santana J. M., Casares J., Muñoz-Darias T., Bauer F. E., Martínez-Pais I. G., Russell D. M., 2016, A&A, 587, A61
Dalton G. et al., 2014, in Suzanne K. R., Ian S. M., Hideki T., eds, Proc. SPIE Conf. Ser. Vol. 9147, Ground-Based and Airborne Instrumentation for Astronomy V. SPIE, Bellingham, p. 91470L
de Jong R. S. et al., 2014, in Suzanne K. R., Ian S. M., Hideki T., eds, Proc. SPIE Conf. Ser. Vol. 9147, Ground-based and Airborne Instrumentation for Astronomy V. SPIE, Bellingham, p. 91470M
Foreman-Mackey D., Hogg D. W., Lang D., Goodman J., 2013, PASP, 125, 306
Gaia Collaboration, 2018, A&A, 616, A10
Gentile Fusillo N. P. et al., 2019, MNRAS, 482, 4570
Gould A., Salim S., 2002, ApJ, 572, 944
Holberg J. B., Oswalt T. D., Sion E. M., McCook G. P., 2016, MNRAS, 462, 2295
Hopkins P. F. et al., 2018, MNRAS, 480, 800
Kollmeier J. A. et al., 2017, preprint (arXiv:1711.03234)

Korol V., Rossi E. M., Groot P. J., Nelemans G., Toonen S., Brown A. G. A., 2017, MNRAS, 470, 1894
Korol V., Koop O., Rossi E. M., 2018, ApJ, 866, L20
Lamberts A. et al., 2018, MNRAS, 480, 2704
Lamberts A., Blunt S., Littenberg T. B., Garrison-Kimmel S., Kupfer T., Sanderson R. E., 2019, MNRAS, 490, 5888
Lau M. Y. M., Mandel I., Vigna-Gómez A., Neijssel C. J., Stevenson S., Sesana A., 2019, MNRAS, 492, 3061
Liu J. et al., 2019, Nature, 7784, 618
Nelemans G., Yungelson L. R., Portegies Zwart S. F., 2001, A&A, 375, 890
Nishizawa A., Sesana A., Berti E., Klein A., 2017, MNRAS, 465, 4375
Rodriguez C. L., Chatterjee S., Rasio F. A., 2016, Phys. Rev. D, 93, 084029
Samsing J., Ramirez-Ruiz E., 2017, ApJ, 840, L14
Sesana A., 2016, Phys. Rev. Lett., 116, 231102
Seto N., 2019, MNRAS, 489, 4513
Speagle J. S., 2019, MNRAS, 493, 3132
Thompson T. A. et al., 2019, Science, 366, 637
Tomczak A. R. et al., 2014, ApJ, 783, 85
Wyrzykowski Ł. et al., 2016, MNRAS, 458, 3012
Zevin M., Pankow C., Rodriguez C. L., Sampson L., Chase E., Kalogera V., Rasio F. A., 2017, ApJ, 846, 82
Zevin M., Samsing J., Rodriguez C., Haster C.-J., Ramirez-Ruiz E., 2019, ApJ, 871, 91

This paper has been typeset from a TEX/LATEX file prepared by the author.